

Calibration of hydrogen atoms measurement by femtosecond two-photon laser induced fluorescence

Andrey Starikovskiy¹, Arthur Dogariu^{1,2}

¹*Dept. of Mechanical and Aerospace Engineering, Princeton University*

²*Dept. of Aerospace Engineering, Texas A&M University*

Abstract

A new calibration method for H-fs-TALIF is proposed, and the ratio of two-photon absorption cross-sections $\sigma^{(2)}$ for atomic hydrogen (H) and krypton (Kr) is determined for the broadband emission of a femtosecond laser system. The obtained estimate of the ratio of two-photon absorption cross-sections $\sigma^{(2)}$ for H and Kr is $\sigma^{(2)}(\text{Kr})/\sigma^{(2)}(\text{H}) = 0.034 \pm 0.006$, which is almost twenty times lower than the values previously obtained using narrowband nanosecond lasers. This difference is explained by the significantly different spectral width of the excitation line, and demonstrates the need for independent calibration of the TALIF measurements in the femtosecond range.

Introduction

TALIF extends the applicability of laser-induced fluorescence (LIF) to light atoms (such as O, N, H) with wavelength transitions in the VUV range by using a two-photon excitation scheme. The advantages of femtosecond TALIF (fs-TALIF) over the traditional nanosecond TALIF technique have recently been reported [1,2]. These include greater excitation efficiency and higher fidelity quenching rate measurements at red-shifted UV wavelengths over a wider range of operating conditions, significantly reduced photolytic interference, and a much higher measurement rate (kHz range). The use of fs- and ps- lasers is particularly useful for TALIF in measuring the effective lifetime of excited levels in highly collisional environments. With fs lasers, excitation can be induced on a shorter time scale than de-excitation by quenching, allowing fluorescence to be detected.

Figure 1 shows the simplified energy diagram of the TALIF processes of atomic hydrogen and krypton. In the case of atomic hydrogen, a two-photon transition from the ground state of the

atom $H(1s^2S_{1/2})$ to the excited state $H(3d^2D_{3/2,5/2})$ takes place at the wavelength $\lambda = 205.08$ nm when irradiated by an intense coherent radiation source. This state is depopulated by collisional and radiative mechanisms. Collisional quenching is highly dependent on the composition and density of the medium in which the measurements are made. Radiative scattering leads to the transition of the excited atom to the $H(2p^2P_{1/2,3/2})$ state with the emission of a quantum at a wavelength of 656.3 nm. In the case of the krypton atom, two-photon excitation of the ground state $Kr(4p^6-1S_0)$ at the wavelength $\lambda = 204.13$ nm leads to the transition of the atom to the excited state $Kr(5p'[3/2]_2)$ followed by radiative transition to the $Kr(5s'[1/2]_1)$ state and emission of a photon at the wavelength of 826.3 nm.

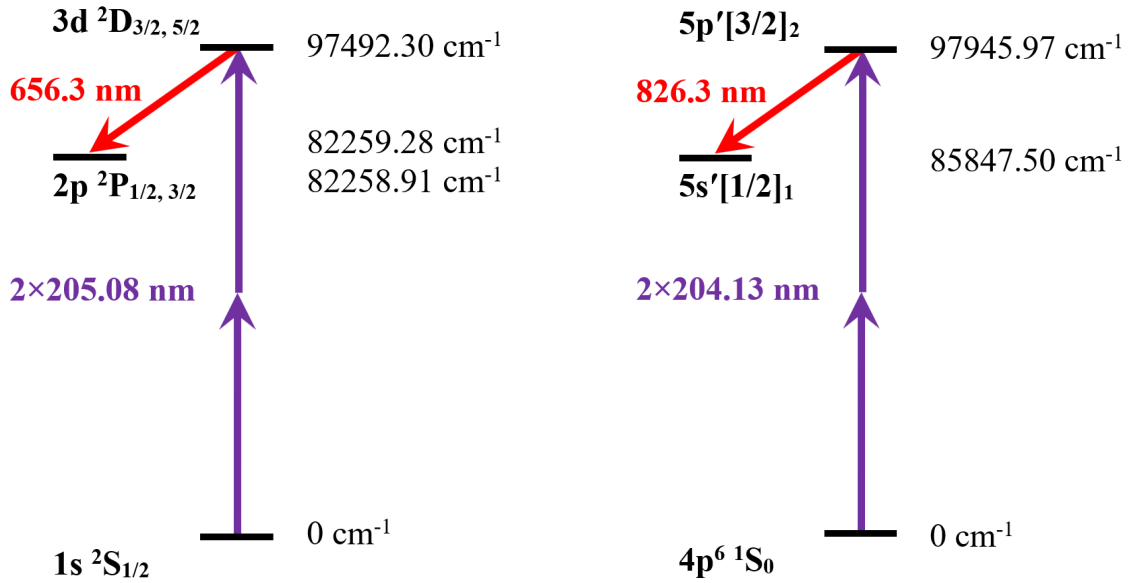


Figure 1. Two-photon excitation energy diagram for TALIF transitions in H (left) and Kr (right). The energy levels are given in cm^{-1} .

With the results of the relative measurements in pure Kr and the gas containing H atoms, the density of the H neutrals, $n(H)$, can be calculated from the measured signals $S(H)$ for hydrogen atoms (at $\lambda = 656.3$ nm) and $S(Kr)$ for krypton atoms (at $\lambda = 826.3$ nm) by knowing the density of the reference gas, $n(Kr)$, as follows [3]:

$$n(H) = n(Kr) \frac{T(Kr) \eta(Kr) \sigma^{(2)}(Kr) a_{2 \rightarrow 3}(Kr) S(H)}{T(H) \eta(H) \sigma^{(2)}(H) a_{2 \rightarrow 3}(H) S(Kr)} kt, \quad (1)$$

where T and η are the wavelength dependent transmission of the optical filters used and the detector efficiency at 656.3 and 826.3 nm, respectively. $\sigma^{(2)}$ are two-photon absorption cross-sections at 205.08 nm for hydrogen and 204.13 nm for krypton. $a_{2 \rightarrow 3}$ is an effective emission coefficient:

$$a_{2 \rightarrow 3} = A_{2 \rightarrow 3} / (A_2 + Q_2) \quad (2)$$

where $A_{2 \rightarrow 3}$ is an Einstein coefficient, A_2 is an inverse radiative lifetime ($A_2 = 1/\tau$), and Q_2 is an inverse quenching lifetime $Q_2 = k_q \times N$, where k_q is a collisional quenching rate. The term kt was added to account for the gating time ($t_2 - t_1$) and delay t_1 (relative to the laser pulse) of the ICCD camera, and could be calculated by integrating the laser signal $I(t)$ at a given wavelength over the gating time with the appropriate delay time:

$$kt = \frac{\int_{t_1}^{t_2} I^2(t) dt (\text{Kr})}{\int_{t_1}^{t_2} I^2(t) dt (\text{H})} \quad (3)$$

Since the two-photon excitation for H and Kr atoms occurs at close wavelengths, tuning the laser to a different frequency does not cause significant changes in beam geometry and focusing. This fact greatly facilitates the absolute calibration of the hydrogen atomic concentration measurements from the known krypton atomic concentration in the calibration experiment.

The main problem of the TALIF technique is that the absolute measurements require the knowledge of all coefficients in equations (1)-(3). Most of the coefficients in equations (1)-(3) could be measured directly from the experimental data with one exception: the ratio of two-photon absorption cross-sections $\sigma^{(2)}$ for H and Kr should be measured separately in the mixture containing the known concentration of H and Kr atoms. These measurements were performed several times using narrow-band nanosecond lasers [3,4]. The concentration of atomic hydrogen in these experiments was measured by adding NO_2 and recording the chemiluminescence resulting from the reaction of H and NO_2 . This procedure led to an uncertainty in the estimated value of the ratio of the two-photon excitation cross-sections of +50% [3].

The value of $\sigma^{(2)}(\text{Kr})/\sigma^{(2)}(\text{H})$ obtained in [3,4] by using two-photon excitation with a narrow-band nanosecond laser (a bandwidth of 0.07 cm^{-1} around 615 nm, [4]) was subsequently used for absolute calibration of hydrogen atom measurements with both narrow-band ns lasers and ps and fs lasers [5-11]. However, femtosecond lasers have a broad emission spectrum and the excitation cross-sections under these conditions should be measured independently. The aim of this work is the independent calibration of the H-fs-TALIF.

H-atoms source

The most difficult problem for the absolute calibration of the H-TALIF is the generation of a known concentration of atomic hydrogen. In [3,4] this problem was solved by adding NO₂ to the gas stream and analyzing the resulting fluorescence. This method is very labor intensive and has significant accuracy limitations [3]. Therefore, in this work we propose to use a low-pressure DC discharge in xenon with a small addition of molecular hydrogen to generate a controlled amount of H atoms. The main idea of using such a discharge as a tool for H-TALIF calibration is the complete dissociation of molecular hydrogen in the xenon plasma. In this case, the energy structure of xenon and atomic hydrogen levels precludes the accumulation of excited states and hydrogen ionization in such a system. A detailed analysis of the kinetics of energy exchange and charge transfer mechanisms in the H₂-H-Xe mixture is given below.

The discharge chamber consists of a long quartz tube surrounded by a grounded aluminum shield (Figure 2). The inner diameter of a discharge tube is $2R = 50$ mm, and the length of the discharge gap from electrode to electrode is $L = 1000$ mm. The electrode system is constructed according to a symmetrical scheme. Both electrodes are made of an aluminum tube with a diameter of $d = 30$ mm and a length of $l = 250$ mm. The working area of the electrodes is $S = 470$ cm². This geometry allows the use of power supply of any polarity and alternating voltage without reducing the efficiency of plasma generation at low gas pressure in the discharge gap. The large electrode area allows operation over a wide range of discharge currents without transition to an anomalous discharge regime that could reduce discharge homogeneity near the electrodes. At a typical voltage $U \sim 600$ V across the discharge cell and total gas pressure $P \sim 75$ mTorr the reduced electric field in the discharge is $E/n \sim 200$ Td. Such a field ensures efficient excitation and ionization of the gas in the discharge. The electrodes are separated from the aluminum shield by dielectric inserts that allow high voltage up to 50 kV to be applied to the system. Direct measurements of voltage and discharge current in the cell were made using high voltage, high frequency probes. The high-voltage power supply TREK-40 has a high internal impedance ($Z = 200$ kOhm) and delivers square-wave alternating current with a frequency of 1 kHz to the discharge cell.

The electrodes have quartz end windows with a diameter of 25 mm. The windows for optical diagnostics of the discharge are placed in an aluminum shield with a step of 150 mm (Figure 2). The vacuum system connections are mounted on the low voltage electrode. The inlet and outlet nozzles are installed asymmetrically and provide continuous gas exchange in the discharge gap

during the experiment by forming a near-wall flow of fresh gas directed into the discharge tube and continuous gas pumping out near the axis of the discharge cell. The vacuum system is equipped with a turbo vacuum pump and allows an initial vacuum in the system down to $P_0 \sim 10^{-7}$ Torr. The gas circulation in the discharge tube allows a complete gas exchange in the tube every 2 seconds. Together with the leakage rate of the vacuum system $\sim 2 \times 10^{-4}$ mTorr/s, this guarantees the relative purity of the mixture inside the discharge tube at the level of 5 ppm at a total pressure of $P = 75$ mTorr.

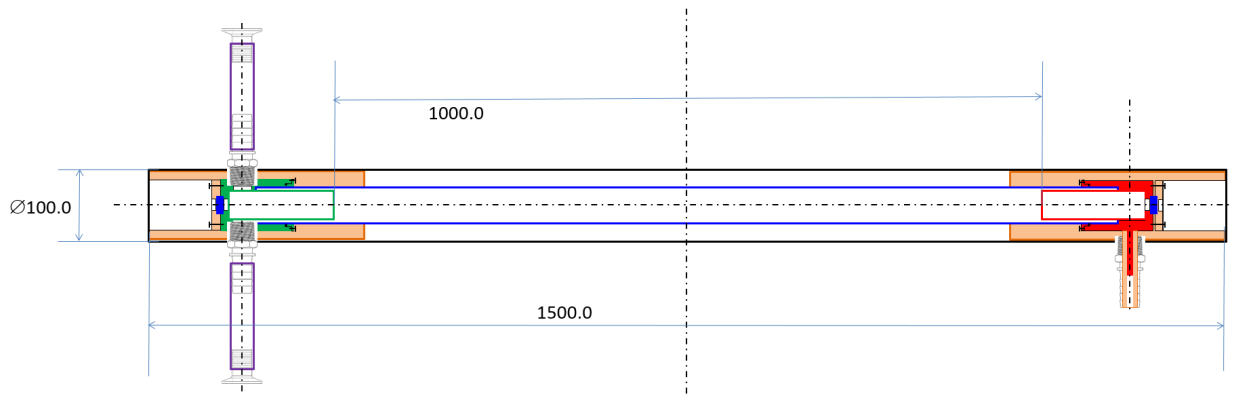


Figure 2. Discharge cell geometry and discharge development in the mixture $\text{Xe} + 112 \text{ ppm H}_2$. $P = 75$ mTorr.

Measurements of the discharge parameters

Figure 3 shows the results of measurements of the current and voltage dynamics in the gap for mixtures with 112 and 200 ppm of H_2 in Xe. It can be seen that the addition of a small amount

of hydrogen does not significantly affect the discharge parameters. The relatively slow recombination of the plasma leads to the preservation of significant ionization as the voltage passes through zero. For this reason, the current follows the voltage almost without delay, reaching a quasi-stationary value at times much shorter than the duration of the voltage pulse plateau (Figure 3).

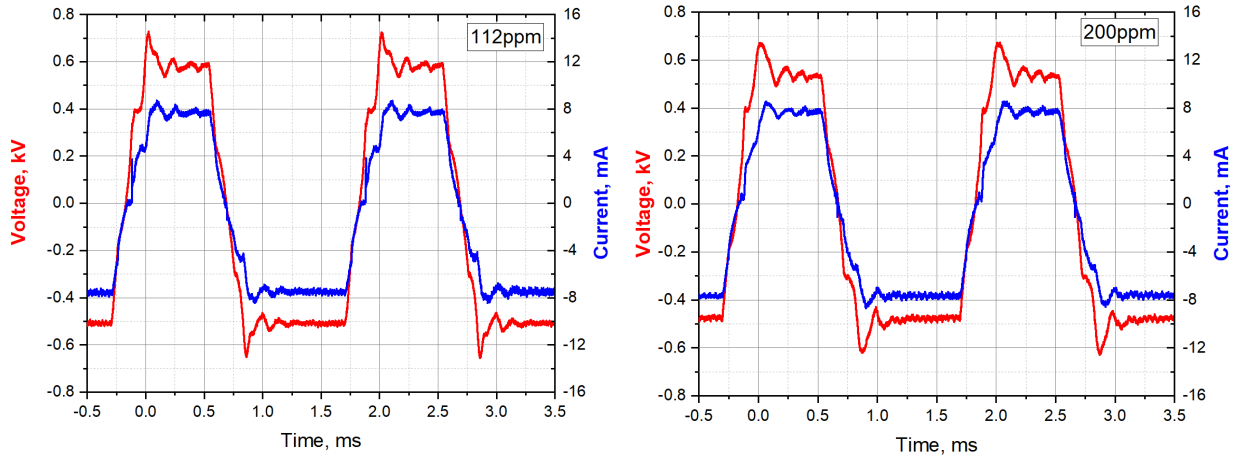


Figure 3. Measured dynamics of voltage and current in the discharge gap. Xe+H₂, $P = 75$ mTorr. Left: mixture Xe + 112 ppm H₂; right: mixture Xe + 200 ppm H₂

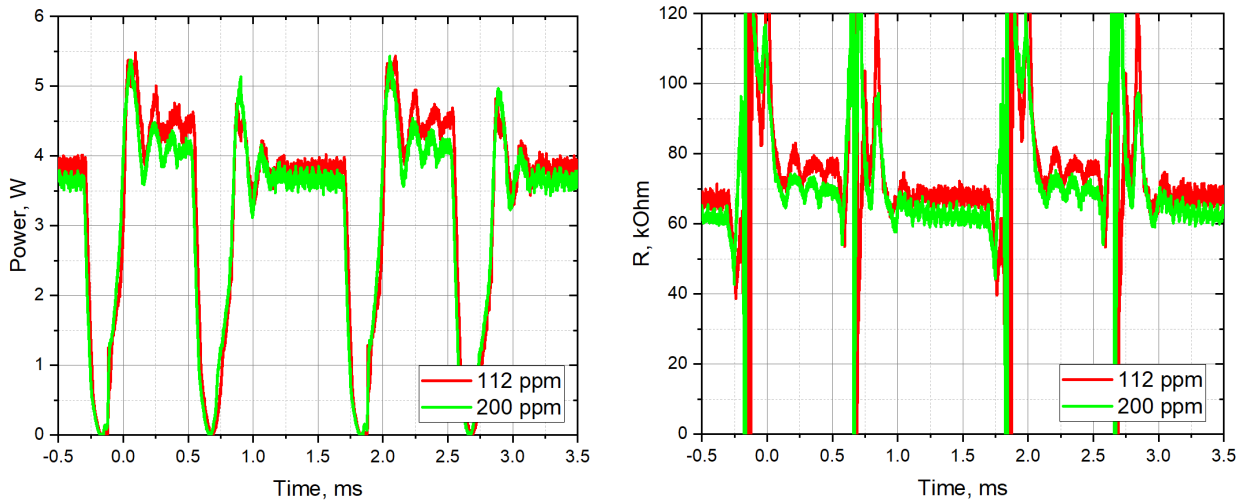


Figure 4. Left: Instantaneous discharge power for different mixtures. Right: Effective impedance of the discharge vs time. Xe+H₂, $P = 75$ mTorr.

Figure 4 shows the discharge power dynamics. The average discharge power in the positive half-wave is about $P \sim 4.5$ W and shows good cycle-by-cycle reproducibility. The power in the negative half-wave also shows the same stability and the average power is about $P \sim 3.8$ W. The

small difference of the discharge power is attributed to the asymmetry of the initial high-voltage waveform (Figure 3). The effective impedance of the discharge also shows great stability and values $R \sim 75 \text{ k}\Omega$ for both investigated mixtures (Figure 4). The relatively low average discharge power keeps the temperature of the discharge tube close to room conditions due to the intensive external air cooling.

Plasmachemical processes in xenon-hydrogen mixtures

The Xe-H₂ system has a number of unique properties that allow us to guarantee both complete dissociation of the molecular hydrogen in the mixture and the absence of significant excitation and ionization of the hydrogen atoms.

One such unique property is the ionization energies of the components (Table 1). Molecular hydrogen has the high ionization energy $E_i(\text{H}_2) = 15.426 \text{ eV}$, atomic hydrogen has an ionization energy of 13.599 eV , and xenon atom has the lowest ionization energy $E_i(\text{Xe}) = 12.13 \text{ eV}$ (Table 1). This hierarchy leads to the fact that no hydrogen ions remain in the system as a result of fast charge transfer reactions – all ions in the system quickly become Xe⁺ ions (reactions (4)-(6)).



The charge transfer reaction rates are of the order of the gas kinetic rates because of the interaction of the ion with the induced dipole. Therefore, it can be argued that there is no accumulation of molecular or atomic hydrogen ions in the system.

Another important feature of the Xe-H pair is the structure of the electronically excited levels of the hydrogen atom and xenon (Table 1). The lower excited states of the hydrogen atom have more energy than the lower levels of xenon. In this case, the collisional depopulation of the excited states of atomic hydrogen becomes very effective:



Table 1. Energy of electronically excited states of H and Xe atoms, ionization, and dissociation of molecular hydrogen [12].

Component	State	Energy, cm ⁻¹	Energy, eV	
Hydrogen molecule	Dissociation threshold	36117.215	4.478	
	Ionization threshold	124418.8856	15.426	
Hydrogen atom	$2p(^2P^0_{1/2})$	82258.921	10.199	
	$2s(^2S_{1/2})$	82258.956	10.199	
	$2p(^2P^0_{3/2})$	82259.286	10.199	
	$3p(^2P^0_{1/2})$	97492.213	12.088	
	$3s(^2S_{1/2})$	97492.223	12.088	
	$3p(^2P^0_{3/2}), 3d(^2D_{3/2})$	97492.321	12.088	
	$3d(^2D_{5/2})$	97492.357	12.088	
	Ionization threshold	109678.774	13.599	
	Xenon atom	$6s[3/2]^0_2$	67068.047	8.315
		$6s[3/2]_1$	68045.663	8.437
$5p^5(^2P^0_{1/2}) 6s^{\uparrow}[1/2]^0_0$		76197.292	9.447	
$6s^{\uparrow}[1/2]^0_1$		77185.56	9.570	
$5p^5(^2P^0_{3/2}) 6p[1/2]_1$		77269.649	9.580	
$6p[5/2]_2$		78120.303	9.686	
$6p[5/2]_3$		78403.562	9.721	
$6p[3/2]_1$		78956.538	9.789	
$6p[3/2]_2$		79212.97	9.821	
Ionization threshold		97834.00	12.13	

The transfer of electron excitation in reactions of the type (7) also takes place with cross-sections close to gas kinetic ones. At the same time, the competition between the processes of settling of electronically excited states of atomic hydrogen by electron impact and the processes of collisional depopulation of such states (8) in collisions with xenon atoms due to the low admixture of atomic hydrogen in the gas (the maximum concentration reaches 400 ppm) and the

low degree of gas ionization in the discharge under these conditions leads to rapid quenching of all electronically excited states of atomic hydrogen.

The excited electronic levels of xenon have energies above 8 eV, which leads to rapid dissociative collisional quenching of these states upon collision with molecular hydrogen, whose dissociation energy is less than 4.5 eV (Table 1).



Since the metastable xenon states in xenon have a long lifetime, the main channel of their depopulation in the gas phase becomes collisions with molecular hydrogen (9)-(10).

Thus, in a mixture of xenon with a small hydrogen addition at low pressure conditions, when three-body processes can be neglected, the main ion is the Xe^+ ion. The excitation of xenon electronic states by electron impact leads to the appearance of an effective dissociation channel of molecular hydrogen. The excitation of atomic hydrogen electronic states in the discharge by direct electron impact is rapidly quenched in collisions with xenon atoms, which have lower electronic state excitation energies.

At low hydrogen concentrations and low mixture pressures, the reverse reaction of gas-phase three-body recombination



which has a rate constant $k_{\text{rec}} \sim 6 \times 10^{-33} \text{ cm}^6/\text{s}$ at $T = 273 \text{ K}$ [13], can be completely neglected, and recombination at the surface of the quartz reactor tube becomes the main channel of hydrogen atom loss.

For a low-catalytic surface of the quartz discharge tube (the surface loss probability of H atoms is less than 2% [14]), diffusion to the surface in the steady-state regime:

$$\frac{1}{[\text{H}]} \frac{d[\text{H}]}{dt} < -D_{\text{H-Xe}}/R^2 \quad (12)$$

The diffusion coefficient of atomic hydrogen in xenon can be estimated to be $P \times D_{\text{H-Xe}} \sim 2 \times 10^{-3} \text{ m}^2 \text{ Torr/s}$ [15]. At the xenon pressure $P = 75 \text{ mTorr}$ used in this work and the inner tube radius $R = 2.5 \text{ cm}$, the diffusion loss rate of atomic hydrogen (12) is at least one order of magnitude smaller than its formation rate in processes (9)-(10) (see also the analysis below).

As a result of this combination of conditions, the small admixture of molecular hydrogen in the $\text{H}_2\text{-Xe}$ mixture in the discharge turns out to be completely dissociated to atomic hydrogen in the ground electron state.

Electron kinetics in xenon-hydrogen discharge

The reduced electric field E/n controls the electron drift velocity v_e in the plasma, the ionization rate, the rate of excitation of the internal degrees of freedom of the molecules by electron impact. Therefore, the E/n parameter is very important in describing the plasma. Figure 5 shows the dynamics of the reduced field during discharge development. These values have been calculated under the assumption of a uniform potential distribution between the electrodes $E = U/L$. This approximation is good enough for the case of a long discharge tube and a large surface of the electrodes, which guarantee a relatively small potential drop in the cathode and anode layers. The positive column of the discharge was uniform in all cases, which was controlled by the intensity of gas excitation along the discharge tube (Figure 2).

Using an estimate of the E/n value in the discharge, we can calculate the electron energy distribution function (EEDF), the mean electron energy, and the electron drift velocity (Figure 6). We used the BOLSIG+ software to calculate the electron ensemble parameters in the two-term approximation of the Boltzmann equation [16]. We used a set of electron impact cross-sections for both Xe and H_2 from the Siglo database [17]. The presence of a small amount of molecular gas (hydrogen) in the mixture insignificantly affects the EEDF and electron swarm parameters. Moreover, as mentioned above, direct electron impact is not the main channel of hydrogen dissociation in such a mixture. Processes (9)-(10) are much faster, and it is these processes that control the rate of hydrogen dissociation in the plasma. Nevertheless, the complete set of excitation, dissociation and ionization processes by electron impact has been considered in the calculations for both xenon and molecular hydrogen.

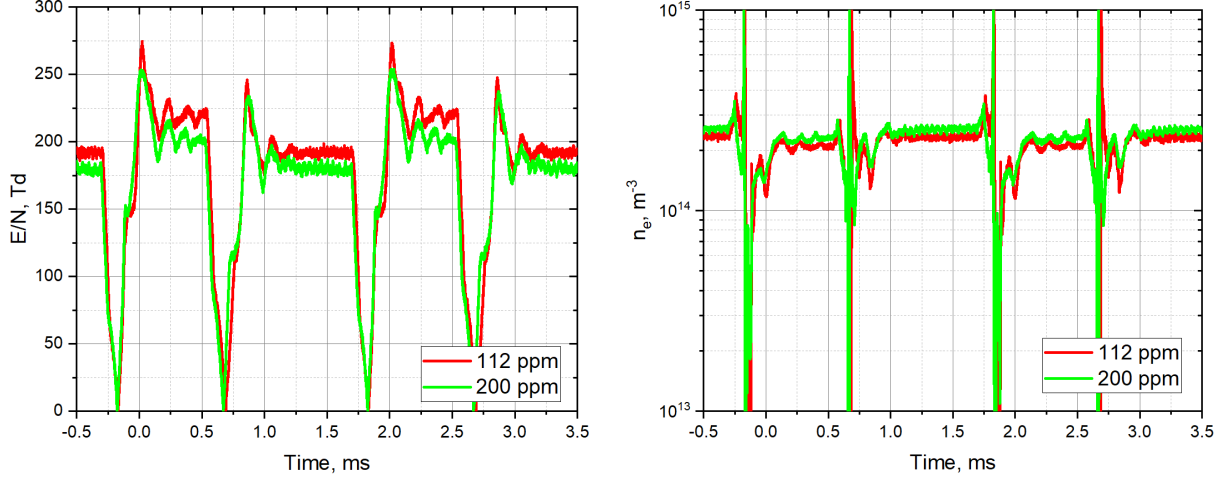


Figure 5. Left: Average reduced electric field in plasma. Right: Electron density in the discharge. Xe+H₂, $P = 75$ mTorr.

In the range of E/n values observed in the experiment ($E/n = 200 \pm 20$ Td, Figure 5), the electron energy distribution function and the electron mobility change only slightly. This allows us to estimate the electron concentration in the discharge with good accuracy using the drift-diffusion approximation. Note that the mobility of electrons in xenon-hydrogen mixture in this region of reduced electric fields also decreases slightly with increasing E/n (Figure 6). The calculated values of the electron drift velocity make it possible to estimate the concentration of electrons in the discharge in a one-dimensional approximation.

In this 1D approximation, we assume that the concentration of electrons and H atoms does not depend on the radius and is constant over the cross-section, and that the voltage drop in the cathode layer is small compared to the positive column of the discharge. Then the total discharge current can be written as

$$I \sim n_e S q_e v_e = n_e S q_e (\mu_e n) (E/n) \quad (13)$$

and

$$n_e \sim I / [S q_e (\mu_e n) (E/n)] \quad (14)$$

The E/n value and the discharge current are known from experimental measurements (Figures 3, 5), the electron mobility is known from calculations (Figure 6). Then the electron concentration in the discharge can be easily estimated using equations (13)-(14). The results of

this estimation are shown in Figure 5. Within the framework of the considered approximation, estimates show that the concentration of electrons in a discharge in a xenon-hydrogen mixture at $P = 75$ mTorr and a total discharge current of about $I \sim 8$ mA is $n_e \sim 2.3\text{-}2.6 \times 10^{14} \text{ m}^{-3}$, and the degree of gas ionization is $[n_e]/[n] \sim 10^{-7}$, which is a characteristic value for DC glow discharges in atomic gases.

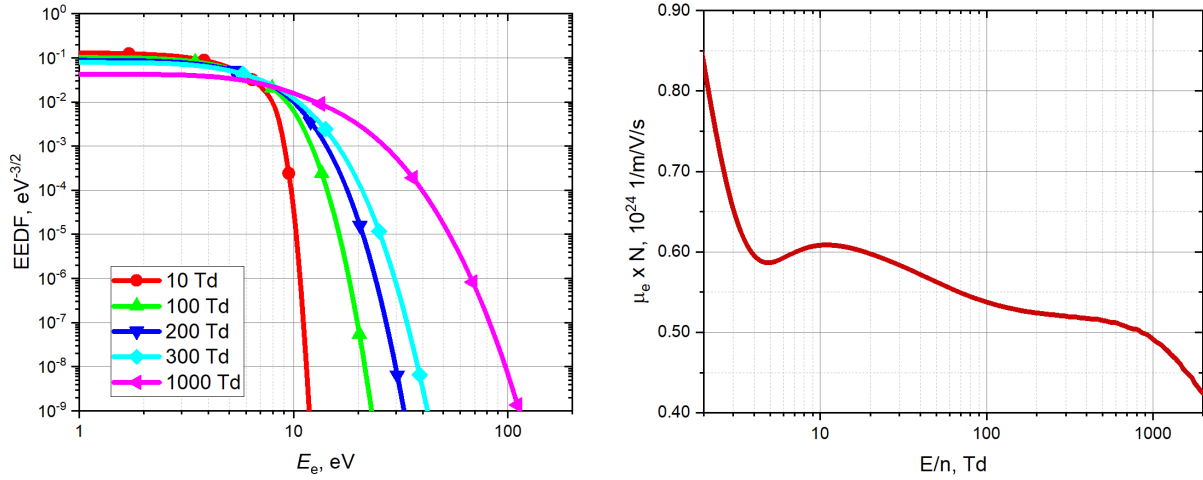


Figure 6. EEDF and electron mobility at different values of the reduced electric field. Mixture Xe + 112ppm H₂.

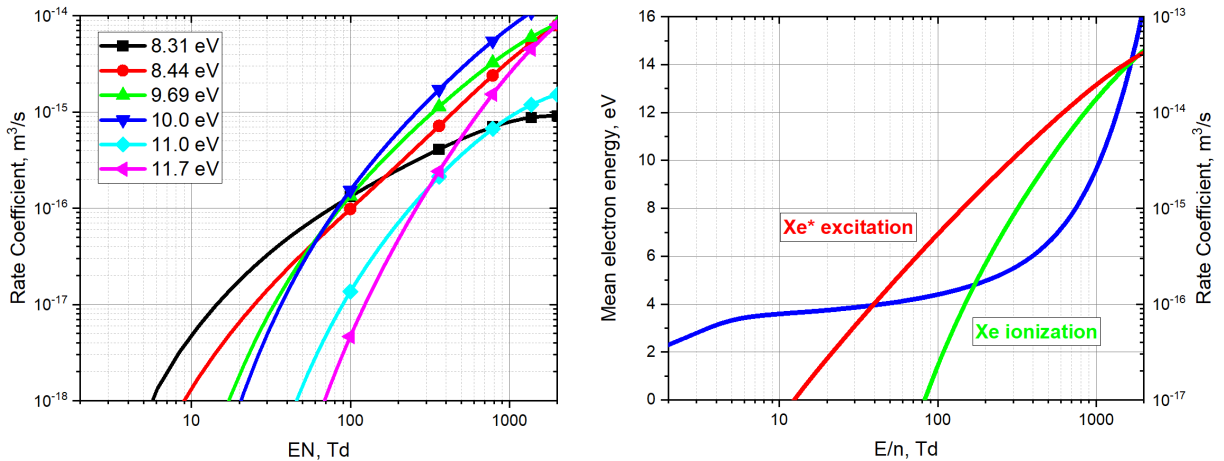


Figure 7. Rate of excitation and ionization of xenon by direct electron impact at different values of the reduced electric field. Mixture Xe₂ + 112 ppm H₂.

Figure 7 shows the rate of excitation and ionization of gas by electron impact. Note that the increase of the reduced electric field value leads to the rapid increase of the excitation and ionization rate coefficients. Within the range of the reduced electric fields corresponding to steady state phase of the discharge (Figure 5, left), the excitation and ionization rate coefficients could vary up to twofold. This behavior is due to the populating of the high-energy tail of the EEDF with increasing electric field. Fortunately, in a steady-state regime, these variations do not lead to significant changes in the electron number density and dissociation degree of molecular hydrogen. Mean energies of electrons in this range of electric fields vary from 5 to 6 eV (Figure 7).

Knowing the electron concentration and the magnitude of the electrical field in the plasma, it is easy to obtain an estimate of the rate of dissociation R_{diss} (reactions (9)-(10)) of molecular hydrogen, the recombination rate R_{rec} (reaction (11)), and the diffusion rate R_{diff} (12) of atomic hydrogen in the plasma (Table 2):

Table 2. Mixture composition and rates of major processes in plasma.

Mixture	[Xe], m ⁻³	[H], m ⁻³	[e], m ⁻³	R_{diss} , m ⁻³ s ⁻¹	R_{rec} , m ⁻³ s ⁻¹	R_{diff} , m ⁻³ s ⁻¹
Xe + 112 ppm H ₂	2.4×10 ²¹	5.4×10 ¹⁷	2.3×10 ¹⁴	8.0×10 ²⁰	8.0×10 ¹²	2.6×10 ¹⁹
Xe + 200 ppm H ₂	2.4×10 ²¹	9.7×10 ¹⁷	2.6×10 ¹⁴	9.0×10 ²⁰	2.6×10 ¹³	4.7×10 ¹⁹

The concentration of atomic hydrogen was calculated assuming complete dissociation of molecular hydrogen. From the comparison of the rates of different processes it is clear that even in this case the rate of formation of atomic hydrogen exceeds many times the rate of its loss in recombination reactions in the gas and on the walls of the discharge chamber. This confirms the earlier conclusion about the complete dissociation of molecular hydrogen in such a system. Thus, under these conditions, the concentration of atomic hydrogen in the ground state in the plasma is determined exclusively by the initial concentration of molecular hydrogen in the initial Xe-H₂ mixture. This conclusion is important from the point of view of calibration of measurement methods, since it makes it possible to produce a known concentration of atomic hydrogen that is practically independent of the kinetic processes in the plasma.

H-fs-TALIF calibration

For the H-fs-TALIF calibration, the discharge in Xe with an admixture of 112 or 200 ppm of H₂ was used (Figure 2). As discussed above, the discharge parameters guarantee a complete dissociation of the hydrogen molecules in the discharge, producing a fixed concentration of H atoms. This allows an independent calibration of the parameters of equation (1). We use these measurements to estimate the ratio of the two-photon absorption cross-sections $\sigma^{(2)}$ for H and Kr.

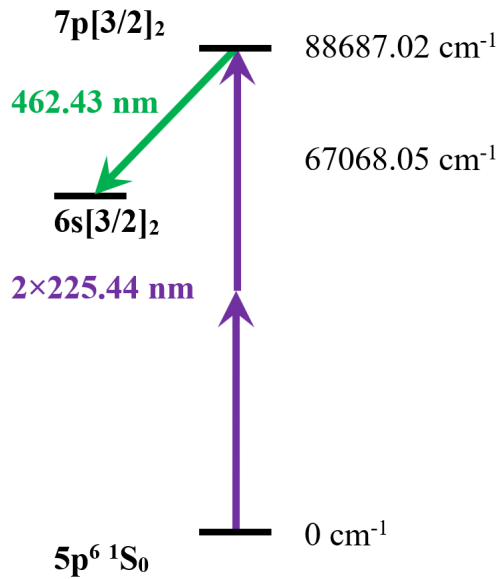


Figure 8. Two-photon excitation energy diagram for TALIF transitions in Xe. The energy levels are given in cm^{-1} .

The TALIF signal generated by neutral H atoms was spatially and temporally resolved by femtosecond two-photon absorption laser-induced fluorescence (fs-TALIF) using a 100-fs amplified laser system capable of generating up to 200 μJ at 205 nm with a repetition rate of 1 kHz. The laser beam is focused on the center of the discharge cell using spherical or cylindrical lenses with a focal length of $f = 600 \text{ mm}$. A fast CMOS camera equipped with a 5 ns gated image intensifier was used to record the H-alpha fluorescence emission at 656 nm for each laser shot. Figure 8 shows the two-photon excitation energy diagram for TALIF transitions in Xe. The significant difference in the excitation wavelength for Xe upper levels compared to the two-photon transitions in hydrogen (Figure 1) guarantees the absence of Xe excitation by the fs-laser pulse and the absence of emission associated with Xe atoms at $\lambda = 656 \text{ nm}$. This fact greatly simplifies the interpretation of H-fs-TALIF data in the Xe-H₂ mixture.

The TALIF signal generated by Kr was measured in the same manner. A two-photon absorption wavelength of 204 nm, and fluorescence emission at 826 nm were used. The signals are evaluated from the intensity of the recorded LIF images. Similar signals are recorded in both H and Kr, and care has been taken to work in the linear regime, before saturation occurs.

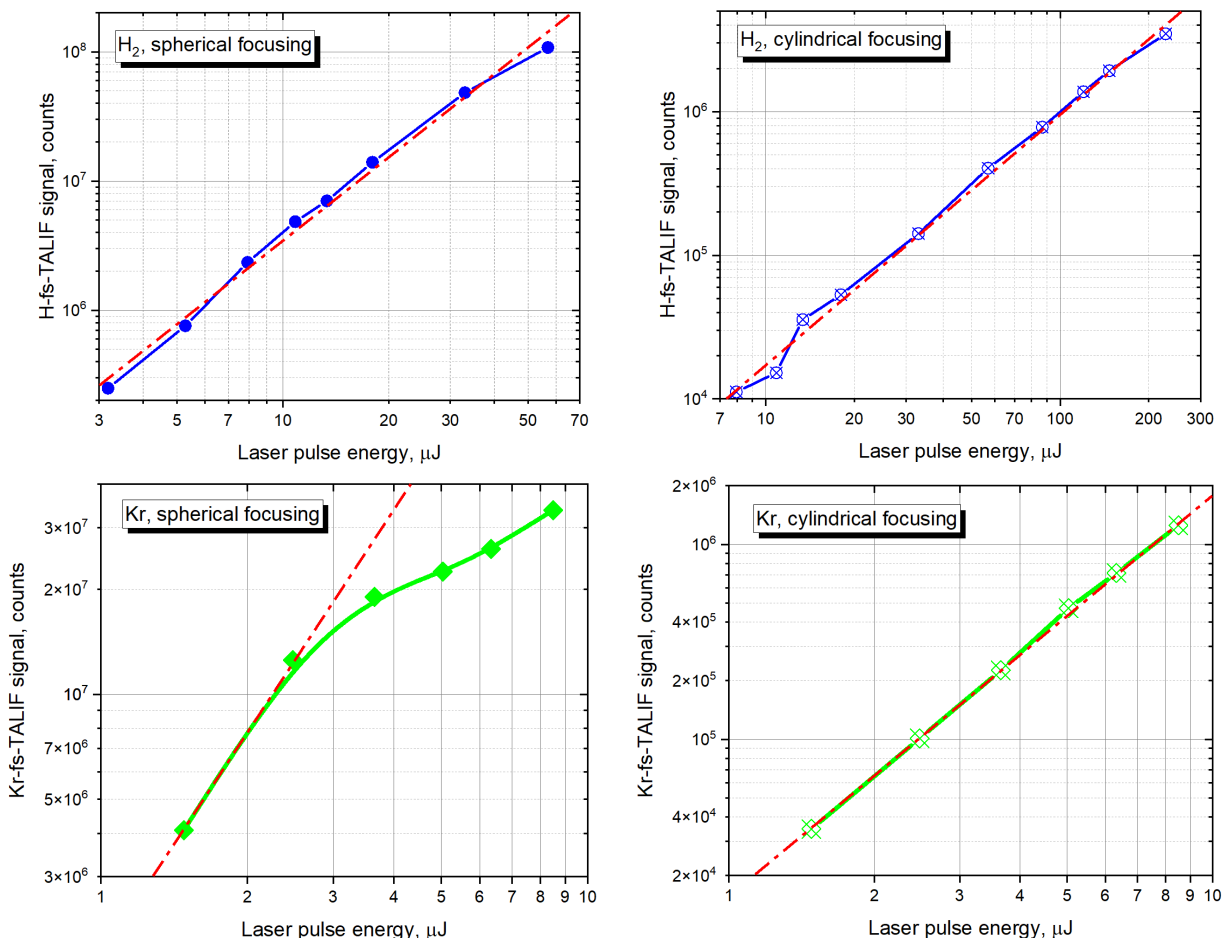


Figure 9. fs-TALIF signals for H (top) and Kr (bottom) as function of pump laser energy for spherical (left) and cylindrical (right) focusing, providing line and sheet TALIF, respectively.

Mixture 115 ppm $H_2 + Xe$, total pressure 85 mTorr (top); pure krypton, total pressure 30 mTorr (bottom). Symbols – measurements, solid lines – data approximation; dash-dot lines – quadratic fits through the point (0;0)

The use of a long discharge cell alleviated the problem of two-photon absorption in the windows. However, it is still necessary to ensure that the TALIF signal is proportional to the density of the species being studied. Also, for proper absolute density calibration, the TALIF signal

must not saturate with the pump laser energy. Since the two-photon absorption is intensity dependent, the energy saturation threshold is expected to be much higher at the lower intensities associated with the cylindrical focusing compared to the spherical focusing. Figure 9 shows the fs-TALIF signals for H (top) and Kr (bottom) obtained by varying the laser energy for both spherical (left) and cylindrical (right) focusing. The dash-dot fits in the log-log plots in Figure 9 follow a quadratic dependence in laser pulse energy, which is owed to the two-photon excitation process in TALIF. Figure 9 demonstrates that cylindrical focusing indeed avoids saturation due to the much lower intensity of the ~ 5 mm wide laser sheet compared to the much higher intensity obtained when focusing with a spherical lens (the focal length was identical for all cases $f = 600$ mm). The H-TALIF measurements were performed with a loading of 85 mTorr of the mixture of xenon and 112 or 200 ppm of molecular hydrogen, which means that the partial pressure of atomic hydrogen produced by the discharge is well below 1 mTorr. For calibration, we use measurements in 100% Kr gas (total pressure in the cell $P = 30$ mTorr, no discharge). Figure 9 shows that at higher pressure the TALIF signal obtained from Kr is much stronger and it saturates faster.

The quadratic fits show that below the saturation threshold the fs-TALIF signals exhibit the two-photon excitation dependence on the laser intensity. For hydrogen atoms, we assume the unsaturated regime to be below $30 \mu\text{J}$ for spherical and below $80 \mu\text{J}$ for cylindrical focusing for hydrogen atoms; for krypton atoms, the unsaturated regime is below $2.5 \mu\text{J}$ for spherical and at least below $10 \mu\text{J}$ for cylindrical focusing. Using these fits, we can calculate the coefficients needed for absolute calibration, provided that the quenching coefficients are also known. We will return to this after describing the lifetime measurements. Figure 9 also gives us the range of energies that are useful for absolute measurements of neutrals. For the following measurements (lifetime and calibration) we have used cylindrical focusing in order to avoid saturation.

To properly calibrate the system as a measure of absolute atomic density, we performed measurements on known densities of Kr, as shown in Figure 10. The Kr-fs TALIF signal was recorded at a sufficiently low laser energy ($3.65 \mu\text{J}$ for cylindrical focusing) to ensure a linear response of the signal. As can be seen from Figure 10, the TALIF signal is proportional to the atomic density, and the slope measured by the linear fit is used to calibrate the TALIF signals. For the absolute calibration of the H atom density using the H-TALIF measurements, it is necessary to know the quenching rates, which depend on the gases and their relative pressures. At lower

pressures, where collisions are minimal, we expect the atomic emission lifetimes to be very little affected, and such lifetimes are easy to measure.

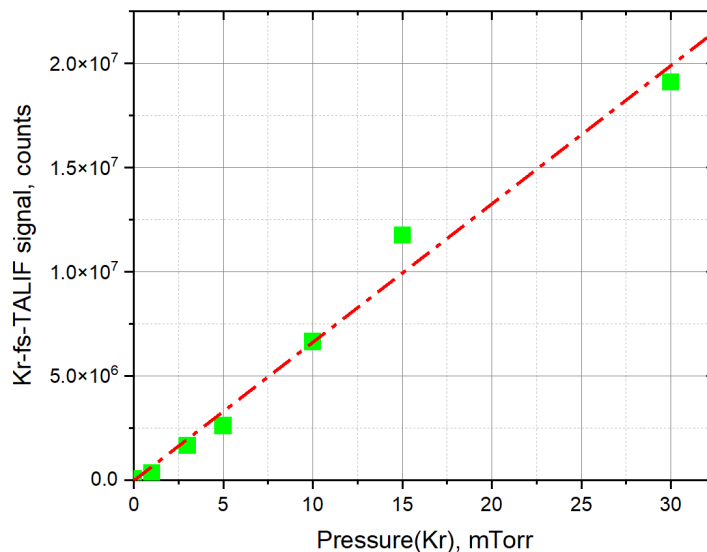


Figure 10. Kr-TALIF signal as function of the Kr pressure. Laser pulse energy 3.65 μJ @ 205 nm. Symbols – measurements, dash-dot line – linear fit.

The H- and Kr- TALIF data presented above were recorded using an integration time of 10 ns. This number was found to be the best balance between collecting enough luminescence (where longer time is better) and being less sensitive to optical background noise (where shorter is better). For lifetime measurements, however, we use the shortest gating time available, which is 1~ns in our setup. With ~1 ns resolution, we can measure the lifetime by varying the delay between the laser pulse and the ICCD gain gate. In Figure 11 we present a series of lifetime measurements performed with H-TALIF (left) and Kr-TALIF (right) for different pressures of the H₂-Xe and Kr gases, respectively.

Figure 11 (left) shows that the lifetime of the H emission does not change significantly going from 28 to 104 mTorr of the 115 ppm molecular hydrogen-xenon mixture, which is to be expected at the low collision rates associated with these pressures. The same is true for Kr, where the measured lifetimes shown in Figure 11 (right) for Kr at 12 and 75 mTorr are very close to the radiative lifetime of Kr. We have also tested krypton under the plasma excitation in order to measure the effect of the ionization (a collisional depopulation of excited states by electron

impact). As shown in Figure 11 (right), the measured lifetimes are in agreement within our experimental error (~ 1 ns), and there is no additional quenching due to ionization, meaning that the discharge itself does not affect our TALIF measurements and thus our estimation of the absolute densities.

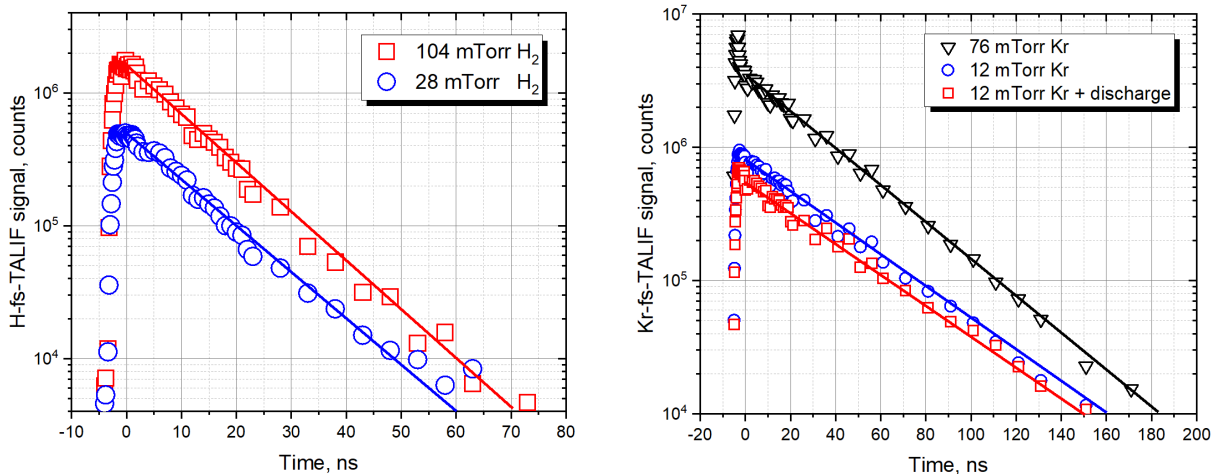


Figure 11. H (left) and Kr (right) emission lifetimes measured with fs-TALIF for several pressures of H₂-Xe mixture and Kr, respectively. Symbols – measurements, lines – emission decay fit.

From these measurements we obtain the lifetimes of 12.5 ns for H and 36.7 ns for Kr, which we will use for our calibration. We can do this with high confidence because the pressures of the gases used in our TALIF measurements (85 mTorr for H₂ and 30 mTorr for Kr) fall within the pressure range shown in Figure 11.

As a result of these measurements, we have estimated the collisional quenching rates k_q ($Q_2 = k_q \times N$, equation (2)) and the radiative lifetime τ ($A_2 = 1/\tau$) for both H and Kr atoms (Table 3). Note that in the pressure range ($P \sim 75$ mTorr) used in the present work, collisional quenching is almost an order of magnitude slower than radiation depopulation of the upper levels and does not affect the concentration dynamics of the excited states. We also estimated the total optical transmission of the detection system T (the interference filter transmittance at the emission wavelength) and the quantum efficiency of the ICCD photocathode η in these spectral intervals.

Thus, we have a complete data set for calculating the value of the ratio of the two-photon absorption cross-sections $\sigma^{(2)}$ for H and Kr, using the known data on the concentrations of atomic

hydrogen, xenon, and krypton in the discharge cell (Table 2). The results of the calculations are shown in Table 4.

Table 3. Parameters for H-fs-TALIF calibration.

	H	Ref	Kr	Ref
λ emission, nm	656.27	[12]	826.30	[12]
λ laser, nm	205.08	[12]	204.13	[12]
$k_q, 10^{-10} \text{ cm}^3 \text{ s}^{-1}$	k(Xe) = 19.8	[3]	k(Kr) = 1.46	[3,18]
	k(Xe) = 19.8	Used in this work	k(Kr) = 1.31±0.065 k(Kr) = 1.46	[10] Used in this work
τ , ns	17.6	[3,18]	34.1	[3,18]
	16.7±0.7	[10]	33.6±1.1	[10]
	10.0±0.5	[4,5]	35.4±2.7	[4,5]
	15.7±1.5	[19]	26.9	[5]
	20.9±0.8	[20]		
	12.5	This work	36.7	This work
$A_{2 \rightarrow 3}, \text{ s}^{-1}$	4.4×10^7	[4]	2.7×10^7	[4]
T	0.90	This work	0.70	This work
η	0.50	This work	0.20	This work

As can be seen from the results presented in Table 4, the ratio of the two-photon absorption cross-sections $\sigma^{(2)}$ for H and Kr when excited by a broadband femtosecond laser differs significantly from the data obtained in [3,4] using a narrowband nanosecond laser, by a factor of almost twenty.

Note that the incomplete dissociation of hydrogen under the conditions of the present work, or the presence of significant amounts of excited hydrogen atoms (if any) would only lead to a decrease in the concentration of atomic hydrogen in the ground state and would further reduce the observed value of $\sigma^{(2)}(\text{Kr})/\sigma^{(2)}(\text{H})$. Thus, the obtained value of the ratio of the two-photon absorption cross-sections $\sigma^{(2)}$ for H and Kr is actually an upper estimate. The accuracy of this estimate is based on the claim of complete dissociation of hydrogen in the Xe-H₂ mixture plasma and the absence of a significant number of hydrogen ions and excited atoms. The above estimates

of the kinetic processes in this system allow us to state that the value $\sigma^{(2)}(\text{Kr})/\sigma^{(2)}(\text{H}) \sim 0.034$ is not only an upper estimate but can be used as calibration data with an accuracy of $\pm 20\%$.

Table 4. The ratio of two-photon absorption cross-sections $\sigma^{(2)}$ for H and Kr.

Method of [H] control	$\frac{\sigma^{(2)}(\text{Kr})}{\sigma^{(2)}(\text{H})}$	Excitation	Ref
Titration with NO ₂	$0.62 \pm 50\%$	ns tunable dye laser, narrow line	[3]
Titration with NO ₂	0.60	ns tunable dye laser, narrow line	[4]
DC discharge in Xe + 112 ppm H ₂ mixture	0.038	100 fs amplified laser system, wide line	This work
DC discharge in Xe + 112 ppm H ₂ mixture	0.033	100 fs amplified laser system, wide line	This work
DC discharge in Xe + 200 ppm H ₂ mixture	0.032	100 fs amplified laser system, wide line	This work

Discussion

The large difference in the ratio of two-photon absorption cross sections $\sigma(2)$ for H and Kr obtained by nanosecond and femtosecond laser excitation is undoubtedly due to the significantly different width of the emission spectrum of the laser systems. Thus, in [4] a laser system based on a pulsed injection-seeded Nd:YAG laser Spectra-Physics/Quanta-Ray GCR-230 and a tunable dye laser Spectra-Physics/Quanta-Ray PDL-3 was used to generate the tunable UV radiation. The dye laser has a bandwidth of 0.07 cm^{-1} at 615 nm, with a presumably smaller bandwidth at the third harmonic, 205nm, used for the H-TALIF. In reference [3], two different narrow line nanosecond dye lasers were used (Spectron SL400 for 205 nm and Radiant Dyes LDL205 for 225 nm).

In our work, we used a frequency-tunable Ti:sapphire laser (Spectra-Physics Solstice) operating at a repetition rate of 1 kHz. The system generates 90 fs pulses with the center wavelength at 820 nm. The measured bandwidth of the fourth harmonic at 205nm was around 1nm, corresponding to about 200 cm^{-1} . The significant differences in spectral width and power density for nanosecond and femtosecond systems dramatically change the excitation cross

sections. Given the much larger bandwidth of the femtosecond laser, the excitation can be considered uniform over the energy distribution of the transitions in the atomic system, regardless of their pressure or temperature broadened profile.

Figure 12 shows the distributions of the effective radiation density of the ns- and fs-laser systems, taking into account the generation of the 3rd harmonic for the ns-system and the 4th harmonic for the fs-system. The Doppler broadening of the line of atomic hydrogen, which has a mass 84 times smaller than that of krypton, significantly increases the effective radiation absorption cross section for the broadband FS system. Thus, the observed difference in the value of the ratio $\sigma^{(2)}(\text{Kr})/\sigma^{(2)}(\text{H})$ for femtosecond and nanosecond laser systems is well explained by the difference in the width of the spectral lines of laser radiation. Another important conclusion that can be drawn from this result is the lower sensitivity of the H-fs-TALIF to temperature changes compared to the nanosecond version of TALIF, since in a wide range of parameters the Doppler broadening of the atomic lines will be significantly smaller than the femtosecond excitation line width. Note also that in the case of e.g. the O-Xe pair (see e.g. the O-fs-TALIF measurements in [1,21-22]), the transition from the nanosecond narrowband system to the broadband excitation in the femtosecond regime will lead to significantly smaller corrections in the calibration due to the significantly smaller mass ratio of xenon and atomic oxygen (~ 8) compared to the Kr-H pair (~ 84).

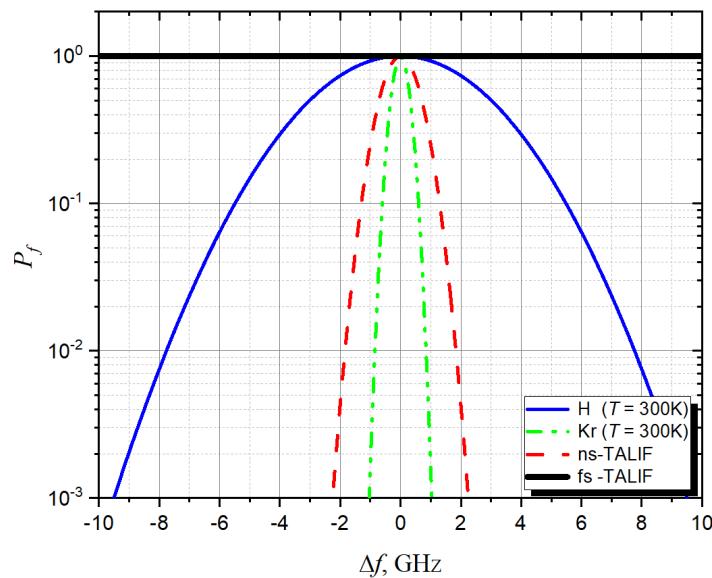


Figure 12. Doppler line broadening and relative distribution of the emission radiation intensity for ns and fs laser systems.

The influence of gas pressure on the value of $\sigma^{(2)}(\text{Kr})/\sigma^{(2)}(\text{H})$ was not investigated in this work. The measurements were performed at low pressures, where the Doppler broadening of the lines significantly exceeds the collisional broadening. The collision broadening is proportional to the collision frequency and depends on the gas density, the thermal velocity of the particles and the cross-section of their interaction $\Delta\omega \sim nv\sigma$. It is obvious that the line broadening for atomic hydrogen and krypton will be significantly different, even if the collisional broadening dominates over the Doppler broadening, due to the large difference in thermal velocities. Note that even in this case, due to the large excitation bandwidth, a relatively low sensitivity of the femtosecond TALIF calibration to changes in the mixture pressure should be expected compared to the nanosecond version of TALIF.

Conclusions

Thus, a variable pressure high voltage plasma discharge test cell has been built for the analysis of H-fs-TALIF capabilities for application in fusion divertors and other relevant environments. The discharge cell allows operation in the pressure range from a few μTorr to tens of Torr, with a gas flow through the cell that ensures continuous gas exchange, which guarantees the absence of impurities.

The plasma parameters in the discharge cell were estimated from the current-voltage characteristics of the discharge. The value of the electric field in the discharge, the concentration of electrons was reconstructed in the 1D drift-diffusion approximation, and on this basis the rates of gas excitation and dissociation in the discharge were estimated. Based on the analysis of detailed kinetics, it is shown that in Xe-H₂ mixtures with low hydrogen content, complete dissociation of molecular hydrogen in the plasma is achieved in the absence of significant ionization and excitation of hydrogen atoms. This fact makes it possible to use such a system as a calibrated hydrogen atom source for various applications.

Based on this H-atom source, a new calibration method for H-fs-TALIF was proposed and the ratio of two-photon absorption cross-sections $\sigma^{(2)}$ for H and Kr was reconstructed. The obtained estimate of the ratio of the two-photon absorption cross sections $\sigma^{(2)}$ for H and Kr for the broadband femtosecond laser excitation is $\sigma^{(2)}(\text{Kr})/\sigma^{(2)}(\text{H}) = 0.034 \pm 0.006$, which is almost twenty times lower than the values obtained with the narrowband nanosecond lasers. This difference is explained by

the significantly different spectral width of the excitation line and demonstrates the need for independent calibration of TALIF measurements in the femtosecond range.

Acknowledgements

This work was partially supported by PPPL Award ROA04736-0004 (Program manager Dr. Ahmed Diallo, Princeton Plasma Physics Laboratory, Princeton) and DOE Award DE-AC02-09CH11466.

References

- [1] J. B. Schmidt, B. Sands, J. Scofield, J. R. Gord, and S. Roy, *Comparison of femtosecond- and nanosecond two-photon-absorption laser induced fluorescence (TALIF) of atomic oxygen in atmospheric-pressure plasmas*. (2017) *Plasma Sources Sci. Technol.* **26**, 055004
- [2] K. Gazeli, G. Lombardi, X. Aubert, C.Y. Duluard, S. Prasanna and K. Hassouni. *Progresses on the use of two-photon absorption laser induced fluorescence (TALIF) diagnostics for measuring absolute atomic densities in plasmas and flames*. (2021) *Plasma* **4** 145–171.
- [3] K. Niemi, V. Schulz-von Der Gathen, and H. F. Dobele. *Absolute calibration of atomic density measurements by laser-induced fluorescence spectroscopy with two-photon excitation*. (2001) *Journal of Physics D: Applied Physics* **34** 5 2330-2335.
- [4] M.G.H. Boogaarts, S. Mazouffre, G.J. Brinkman, H.W.P. van der Heijden, P. Vankan, J.A.M. van der Mullen, D.C. Schram and H.F. Döbele. *Quantitative two-photon laser-induced fluorescence measurements of atomic hydrogen densities, temperatures, and velocities in an expanding thermal plasma*. (2002) *Rev. Sci. Instrum.* **73** 73
- [5] S. Schröter. *Reactive oxygen and hydrogen species generation in radio-frequency atmospheric pressure plasmas*. (2017) PhD Thesis. University of York.
- [6] S.A. Steinmetz, A.T. DeLaRiva, C. Riley, P. Schrader, A. Datye, E.D. Spoerke, C.J. Klierer. *Gas-phase hydrogen-atom measurement above catalytic and noncatalytic materials during ethane dehydrogenation*. (2022) *J. Phys. Chem. C.* **126** 3054–3059.
- [7] A. Dogariu, S.A. Cohen, P. Jandovitz, S. Vinoth, E.S. Evans, C.P.S. Swanson. *A diagnostic to measure neutral-atom density in fusion research plasmas*. (2022) *Rev. Sci. Instrum.* **93** 093519

- [8] J.B. Schmidt, W.D. Kulatilaka, S.Roy, K.A. Frederickson, W.R. Lempert and J.R. Gord. *Fs-TALIF imaging of atomic species in non-equilibrium plasmas at moderate pressures*. (2014) Imaging and Applied Optics. Laser Applications to Chemical, Security and Environmental Analysis Seattle, Washington.
- [9] J.B. Schmidt, W.D. Kulatilaka, S.Roy, K.A. Frederickson, W.R. Lempert, J.R. Gord. *Femtosecond TALIF imaging of atomic hydrogen in pulsed, non-equilibrium plasmas*. (2014) AIAA SciTech Forum. National Harbor, Maryland.
- [10] J.B. Schmidt, S. Roy, W.D. Kulatilaka, I. Shkurenkov, I.V. Adamovich, W.R. Lempert, J.R. Gord. *Femtosecond, two-photon-absorption, laser-induced-fluorescence (fs-TALIF) imaging of atomic hydrogen and oxygen in non-equilibrium plasmas*. (2017) J. Phys. D: Appl. Phys. **50** 015204
- [11] C. Winters, Z. Eckert, Z. Yin, K. Frederickson, I.V. Adamovich. *Measurements and kinetic modeling of atomic species in fuel-oxidizer mixtures excited by a repetitive nanosecond pulse discharge*. (2018) J. Phys. D: Appl. Phys. **51** 015202
- [12] A.A.Radtsig, B.M. Smirnov. *Handbook of Atomic and Molecular Physics*. (1980) Moscow. Atomizdat. 240 pp.
- [13] V.H. Shui, J.P. Appleton. *Gas-phase recombination of hydrogen. A comparison between theory and experiment*. (1971) J. Chem. Phys. **55** 3126–3132
- [14] X.Yang, D.Kogut, L.Couëdel, T.Angot, P.Roubin, J-B. Faure, G.Cartry. *TALIF measurements of hydrogen and deuterium surface loss probabilities on quartz in low-pressure high-density plasmas*. (2021) Plasma Sources Sci. Technol. **30** 015013
- [15] *Tables of physical quantities. Handbook*. (1976) Ed: I.K. Kikoin. Moscow. Atomizdat. 1008 pp.
- [16] BOLSIG+ *Electron Boltzmann equation solver*. <http://www.bolsig.laplace.univ-tlse.fr>
- [17] SigloDataBase-LXCat-04. https://us.lxcat.net/data/set_databases.php
- [18] H.F. Döbele, T. Mosbach, K. Niemi, V. Schulz-von der Gathen. *Laser-induced fluorescence measurements of absolute atomic densities: concepts and limitations*. (2005) Plasma Sources Sci Technol **14** S31
- [19] B.L. Preppernau, K. Pearce, A. Tserepi, E. Wurzburg, T.A. Miller. *Angular momentum state mixing and quenching of $n = 3$ atomic hydrogen fluorescence*. (1995) Chem Phys **196** (1–2) 371-381.

- [20] J. Bittner, K. Kohse-Hoinghaus, U. Meier and Th. Just. *Quenching of two-photon-excited H(3s, 3d) and O(3p ³P_{2,1,0}) atoms by rare gases and small molecules.* (1988) Chem Phys Lett **143** (6) 571-576.
- [21] J.D. Scofield, J.R. Gord, J.B. Schmidt, S.Roy, B.Sands. *Comparison of femtosecond- and nanosecond-two-photon-absorption laser induced fluorescence (TALIF) of atomic oxygen in atmospheric pressure plasmas.* (2016) Report AFRL-RQ-WP-TR-2016-0118. Air Force Research Laboratory. Aerospace Systems Directorate. Wright-Patterson Air Force Base. OH 45433-7541
- [22] J.B. Schmidt, B.L. Sands, W.D. Kulatilaka, S. Roy, J. Scofield, J.R. Gord. *Femtosecond, two-photon laser-induced-fluorescence imaging of atomic oxygen in an atmospheric-pressure plasma jet.* (2015) Plasma Sources Sci. Technol. **24** 032004.